Charmonium photoproduction with GlueX

Alexander Austregesilo, Eugene Chudakov, Sean Dobbs, Sergey Furletov, and Lubomir Pentchev

(Dated: May 19, 2023)

Abstract

We propose to improve the precision of the measurements of exclusive J/ψ photoproduction near threshold with the GlueX experiment by introducing an additional pion-suppression detector, a Transition Radiation Detector based on GEM amplification, or GEM-TRD. We discuss the importance of the physics of charmonium photoproduction and the need for precise data in the near-threshold region. We describe the new detector and, based on existing GlueX data, we demonstrate that it will significantly reduce the systematic uncertainties of these measurements.

I. EXECUTIVE SUMMARY

The measurements of J/ψ exclusive photoproduction near threshold [1] using GlueX data have sparked intense theoretical interest in using this process as a tool to study the gluon structure of the proton: the gluon Generalized Parton Distribution (GPD), the mass radius of the proton, and the anomalous contribution to the proton mass. However, such an ambitious program requires detailed studies of the reaction mechanism to verify the assumptions used in theoretical models to interpret the data. In the latest GlueX results [2] we observe possible structures in the $8.6 - 9.5$ GeV region in the total cross section, and an enhancement of the differential cross section for these energies towards t_{max}. These two observations, if statistically significant, would indicate contributions beyond a simple t-channel exchange that would obscure the extraction of the proton's gluonic properties. Such contributions would also obscure the search in this process for s-channel excitations, such as the LHCb pentaquark states, P_c^+. Recently JPAC published fits of our data with several phenomenological models: gluon exchange, open-charm exchange, and s-channel resonances [3]. As with the present uncertainties there is no statistically significant preference to any of these models, precise measurements would allow us to disentangle the possible reaction mechanisms which is critically important to study the mass structure of the proton.

We propose to substantially improve the precision of the charmonium photoproduction measurements by running for 100 PAC days with an additional pion-suppression detector, a Transition Radiation Detector based on GEM amplification, or GEM-TRD. As an independent low-mass detector, the GEM-TRD will allow us to study the forward calorimeter pion suppression efficiency. The GEM-TRD will significantly reduce the pion contamination for the Bethe-Heitler process used to normalize the J/ψ cross sections, and will allow for a better determination of the overall efficiency through comparisons with QED calculations.

With this Letter of Intent, we seek the PAC's feedback on the importance of the new detector for the charmonium physics and taking into account the PAC's opinion we plan to come with a full proposal next year. The proposed measurements can be done in parallel with the GlueX program and will benefit significantly from the proposed intensity increase of the GlueX experiment [4]. The charmonium studies with GlueX, including first ever evidence for C-even charmonium photoproduction, are playing important role in justifying a possible future JLab energy upgrade.

II. INTRODUCTION

Over the past several years there has been a renewed interest in studying near-threshold J/ψ photoproduction as a tool to experimentally probe important characteristics of the proton based on its gluon content, most importantly to get insight in the origin of the nucleon mass. Several theoretical approaches have been used to connect heavy quarkonium photoproduction to the gluon-nucleon interaction and to further study the mass properties of the proton.

The vector meson dominance (VMD) model is used to relate the J/ψ photoproduction, $\gamma p \to J/\psi p$, to the $J/\psi p \to J/\psi p$ elastic interaction [5]. Once such a connection is established, J/ψ acts as a probe of the gluonic structure of the proton, in much the same way as electrons are used in ep elastic scattering to study the electro-magnetic properties of the nucleon. The main difference is that, due to the heavy mass of the charm quark, J/ψ interacts with the proton predominately through gluon exchange. Thus, we can access important properties of the proton that are not accessible via much more popular electromagnetic probes. It was shown in [5] that close to threshold, the forward differential cross section of the $J/\psi p \to J/\psi p$ reaction contains information about the anomalous contribution to the mass of the proton, that is generated by the gluonic fields.

An important QCD approach to describing this process is to assume factorization, with the gluon GPD and the J/ψ wave function on one side, and the perturbative hard scattering between the gluons and the charm quarks on the other side. For high energies and low $|t|$ values, it was demonstrated in Ref.[6] that the factorization is valid in leading (LO) and next-to-leading (NLO) order. An important study was done in Ref.[7], where they have shown that in the case of the heavy quark mass limit, the factorization is valid down to the threshold along the t_{min} line. Even more, it was shown [7, 8] that due to the high skewness (ξ) values near threshold, the process is dominated by 2^{++} graviton-like exchange, allowing to indirectly study the mass properties of the proton. We see a good agreement of the total J/ψ photoproduction cross section measured at GlueX with the GPD calculations as shown in Fig.1. This indicates that our measurements can strongly constrain the relevant gluon GPD functions.

Within the gluon exchange mechanism framework, the t-dependence of the differential cross section is defined by the proton gluonic form factors. In Refs.[7, 13–17] it is argued

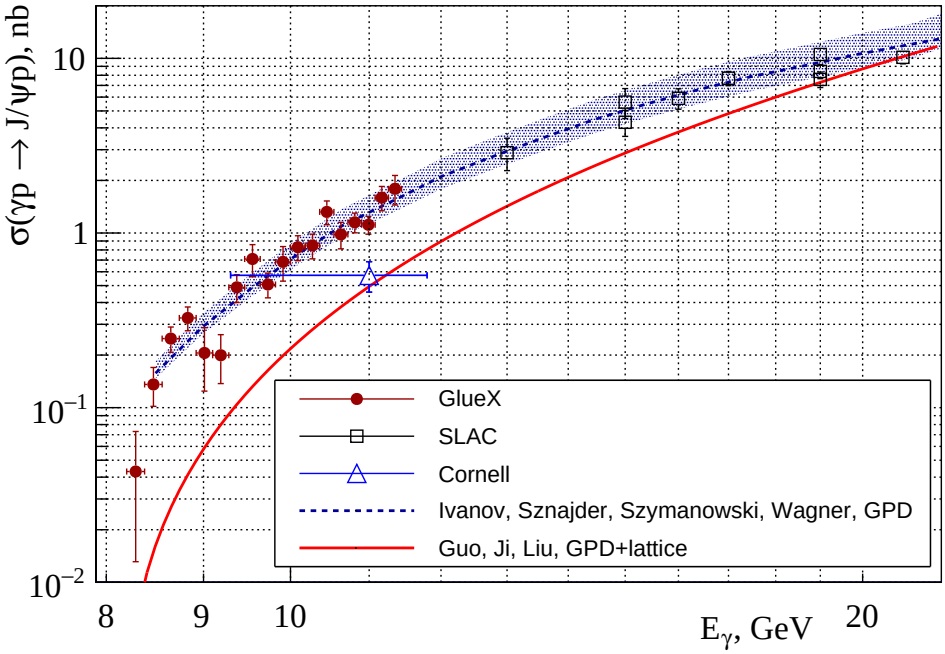

FIG. 1: Comparison of the GlueX J/ψ total cross-section to the SLAC [9] and Cornell [10] data and two QCD theoretical calculations in the two-gluon exchange factorization model (in LO) from Ref.[11] and from Ref.[7], the latter using gravitational form factors from lattice calculations [12].

that these are nothing else but the gravitational form factors. These form factors can be parametrized with a dipole function [12, 18]. In Fig.2 we fit the GlueX results [2] for the differential cross sections, $d\sigma/dt(t)$, in three slices of the beam energy, with a dipole function. For the lowest energy we exclude the high-t region,which will be discussed further below. The mass scale parameter, m_s, that defines the t-slope in our data is generally in a good agreement with the lattice calculations for the $A_g(t)$ gravitational form factor [12]. However, this view is not universally shared. Ref.[19] directly calculates the Feynman diagrams of near-threshold heavy quarkonium photoproduction at large momentum transfer and finds that there is no direct connection between the t-dependence of the differential cross sections and the gravitational form factors.

The authors of Ref. [20] propose an alternative mechanism of J/ψ photoproduction with a dominant exchange of open-charm channels $\Lambda_c\bar{D}$ and $\Lambda_c\bar{D}^*$ in box diagrams. We show the total cross section results of this model in Fig. 3, and find good qualitative agreement with our measurements. In particular, in the data we see structures peaking at both the $\Lambda_c\bar{D}$ and $\Lambda_c\bar{D}^*$ thresholds that can be interpreted as the cusps expected with this reaction mechanism.

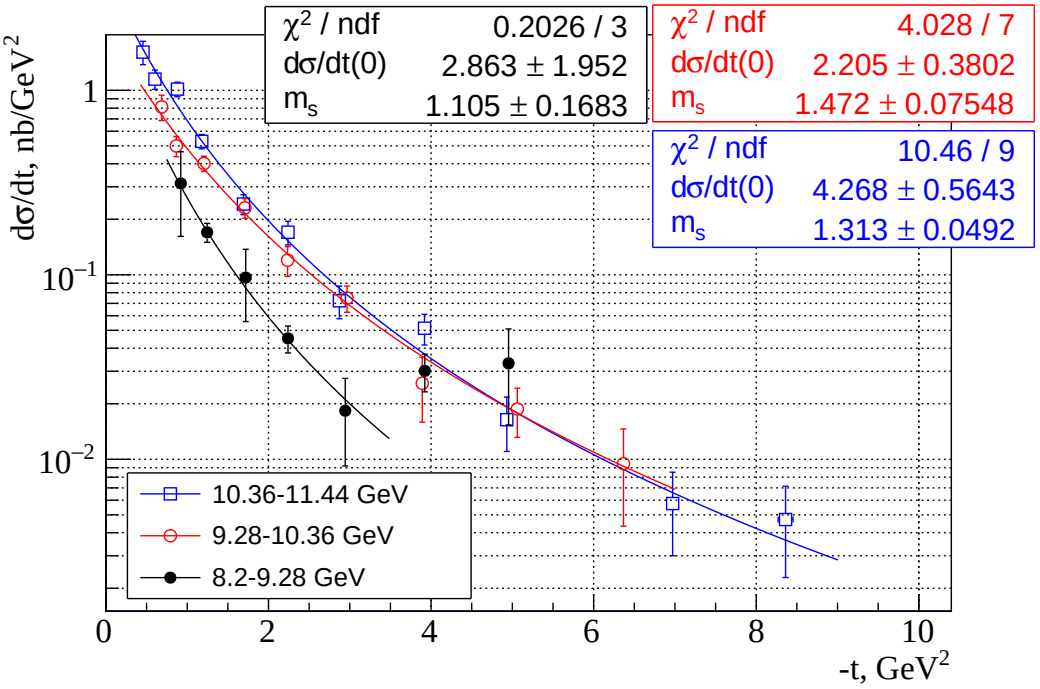

FIG. 2: The differential cross sections for the three energy slices fitted with $[d\sigma/dt(0)]/(1-t/m_s^2)^4$, where the cross section at $t=0$, $d\sigma/dt(0)$, and the mass scale, m_s, are free parameters.

The shape of the dip in the data can be interpreted within the errors as a step between the two thresholds, as suggested from the theoretical curves. However, the exchange of heavy hadrons in this model implies a very shallow t-dependence in the differential cross sections. This is not supported by the steeply falling cross sections we observe, as shown in Fig. 2. Thus, our results for differential cross sections do not support a dominant contribution from these open charm exchanges, although the enhancement at high t observed for the lowest beam energy region is consistent with a possible contribution from these exchanges.

We conclude that in order to relate the near-threshold J/ψ photoproduction to the mass properties of the proton, a better understanding the reaction mechanism is required. Furthermore, understanding the contribution of any processes besides gluon exchange to J/ψ photoproduction is crucial for the search for the photoproduction of the LHCb P_c^+ pentaquark candidates [21, 22]. The P_c^+ states can be produced in the s-channel of the $\gamma p \to J/\psi$ reaction [23–26]. At same time the open-charm exchange mentioned above acts as an s-channel process and can result in similar structures in the total and differential cross sections. In an attempt to disentangle the contributions from the different mechanisms, in a recent JPAC

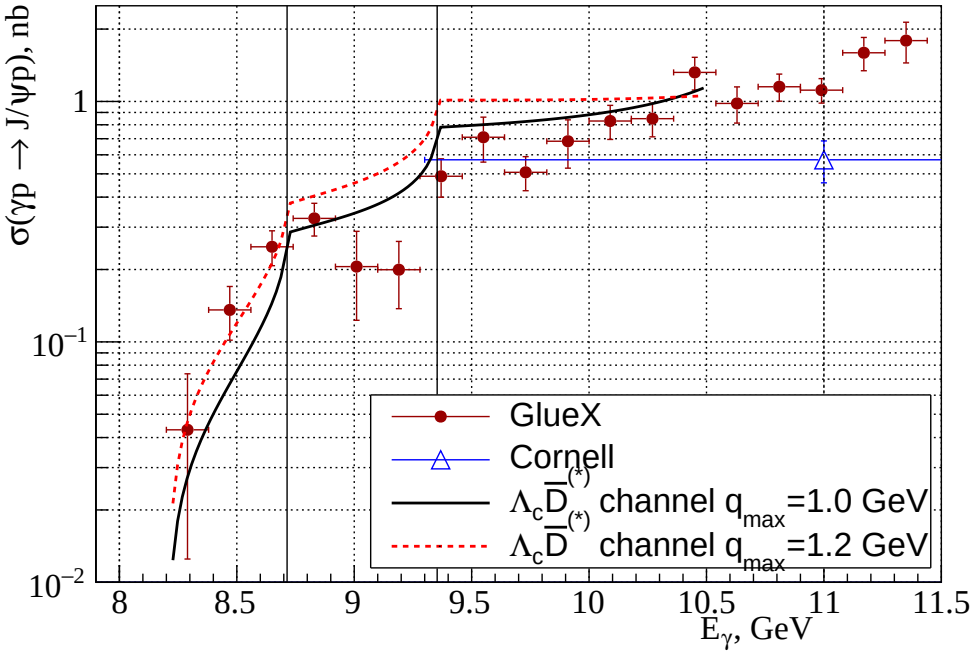

FIG. 3: Comparison of the GlueX J/ψ total cross-section to open charm calculations [20] (for two values of q_{max} parameter). Shown are $\Lambda_c\bar{D}$ and $\Lambda_c\bar{D}^*$ thresholds as vertical lines. For the GlueX points, the error bars shown are the quadrature sum of the statistical and systematic errors.

work [3] they fit our data with four phenomenological model that include combinations of gluon exchange, open-charm exchange, and s-channel resonances. The data from the other JLab experiment, J/ψ-007 [27] are included in the fit assuming common normalization of the two data sets. The fit results show that severe violations of the factorization and the VMD model are not excluded, and that the open-charm exchange may have non-negligible contribution. However all these conclusions are not statistically significant.

Measurements with improved precision at GlueX are crucial to developing this better understanding of J/ψ photoproduction. We will discuss in detail the use of the GEM-TRD detector and its effect on reducing the systematic uncertainties of these measurements. To demonstrate this, throughout this document, we use real data from Phase-I of the GlueX experiment plus the engineering run in 2016, as used in our recent paper [2]. These data correspond in total to a little more than 100 PAC days, however during the Phase-I running the intensity of the photon beam gradually increased by a factor of two to the beam intensities that are assumed in the studies presented below. We also note that the current Phase-II run uses a beam intensity nearly a factor 2 larger than that of Phase-I. Therefore,

it is fair to use the presented results as realistic upper limits of the expected uncertainties when running for 100 PAC days under current GlueX conditions.

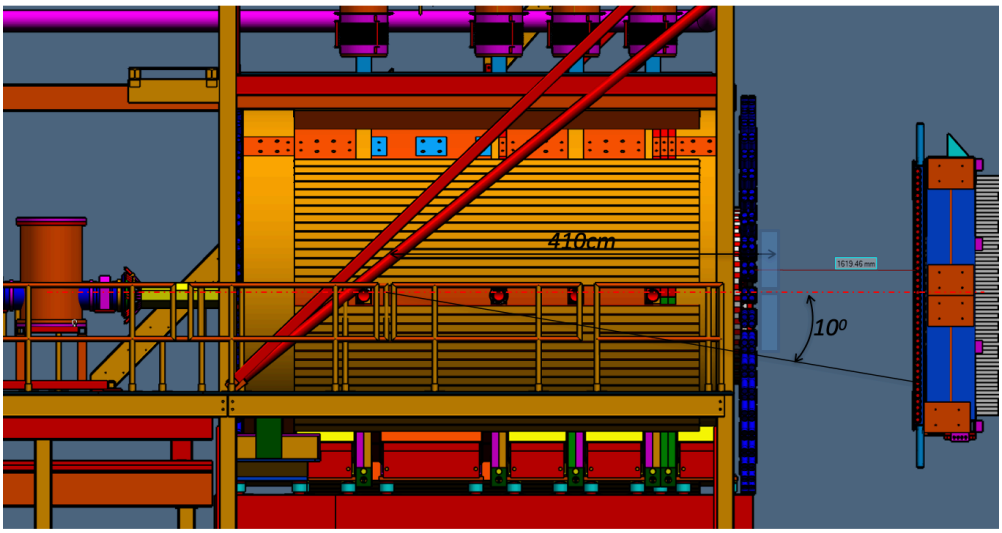

FIG. 4: Side view showing the approximate position of the proposed GEM-TRD detector (light blue boxes), at 410 cm downstream of the target, covering 86% of the forward GlueX acceptance of $\sim 10^\circ$ polar angle. The DIRC detector is not on the plot.

III. THE GEM-TRD DETECTOR

The GEM-TRD will be placed in the forward region of the GlueX detector just at the downstream face of the solenoid, in front of the DIRC and FCAL, as shown in Figs. 4,5. It will consists of two separate chambers, each providing 1392×528 mm^2 sensitive area. The frames of the chambers holding the front-end electronics will be outside of the acceptance (Fig. 5).

The detector consists of: a radiator layer 15 cm thick, a 2 cm drift volume, and a GEM stage combined with a readout board. The principle of operation is illustrated in Fig.6a. The Transition Radiation (TR) photons in the keV region produced by the electrons in the radiator are absorbed by the Xe gas mixture in the drift volume emitting electrons that drift to and are amplified by the GEM. The signals are read out from X- and Y-strips on the readout board. The horizontal strips are separated in the middle and read out from the left and right side of the chambers (Fig. 5). The strip pitch is 1 mm, resulting in $2,448$ electronic channels per chamber, or $4,896$ in total. The signals are amplified on-

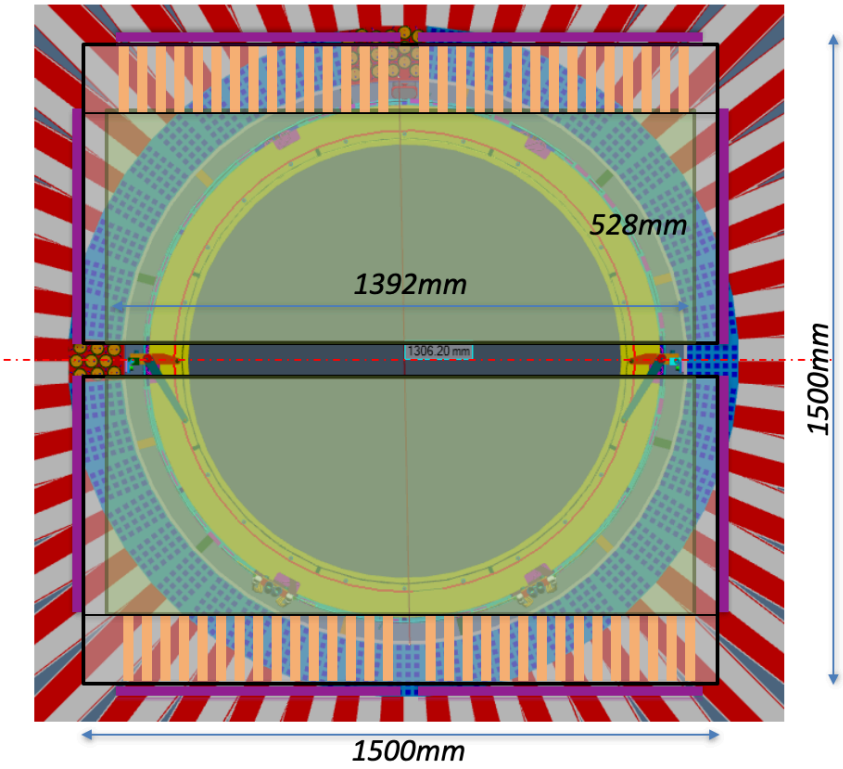

FIG. 5: Front view of the GEM-TRD detector placed at the face of the solenoid magnet. It consists of two separate chambers with 1392×528 mm^2 sensitive area. All the frames holding the front-end electronics (purple thick lines) of sizes $\sim 1500 \times 1500$ mm^2 are outside of the GlueX forward acceptance.

board and then digitized with flash ADCs. We assume as a default configuration using the same electronics as for the GlueX drift chambers: GASII [28] preamps and flashADC-125 [29], however an alternative better option is being discussed. Thus, we record the energy deposition as function of the drift distance along the track. Note the different profile for the TR photons that are absorbed predominately at the entrance of the detector, and the charged particle ionization that has a more uniform distribution, see Fig.6b. At the same time such detector works as a Time Projection Chamber, allowing the reconstruction of the track segment within the drift volume.

The main parameters of the GEM-TRD detector are given in Table I. They are based on tests with small prototypes (10×10 cm^2) done during the past several years, and are preliminary. Further optimization of the detector will be done with the large-scale GEM-TRD prototype that has been recently built. This prototype covers a quarter of the final detector (Fig.7).

Studies with small (10×10cm^2) prototypes have been done during 2018-2022 [30]. They

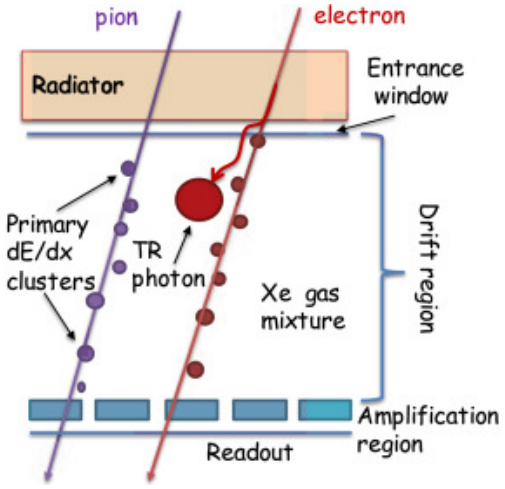

(a) GEM-TRD principle

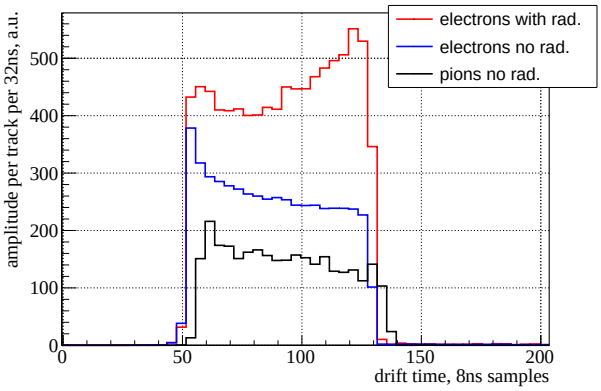

(b) Amplitude profiles for electrons with and without radiator and pions; data from studies with small prototypes

FIG. 6

parameter	value	comment
sensitive area	$2 \times (1392 \times 528\ \mathrm{mm}^2)$	two separate chambers
frame-free area	$1500 \times 1500\ \mathrm{mm}^2$	except some minimal support
distance from the target	4100 mm	
forward acceptance coverage	86%	for e^+e^- invariant mass > 1.2 GeV
radiator thickness	150 mm	
drift volume thickness	21 mm	
total detector thickness	$< 4\%$ R.L.	
drift field	1.5 kV/cm	
gas mixture	Xe/CO_2 90/10	
maximum drift time	800 ns	
gas amplification	$\sim 5.10^4$	
expected pion suppression factor	10	at 90% efficiency, based on studies with small prototypes
strip types	X and Y	on the same layer with capacitive coupling
strip pitch	1 mm	
x,y position resolution	150 μm	
z position resolution	250 μm	using drift time
readout channels	4,896	2,448 per chamber
GASII pre-amps (24 channels)	204	102 per chamber
GASII amplification	2.4 mV/fC	
flashADC-125 (72 channels)	68	34 per chamber
VXS crates	5	

TABLE I: Main parameters of the GEM-TRD detector.

were performed both with electrons obtained from one of the Pair Spectrometer arms, and with pions in the forward GlueX acceptance, downstream of the magnet and in front of

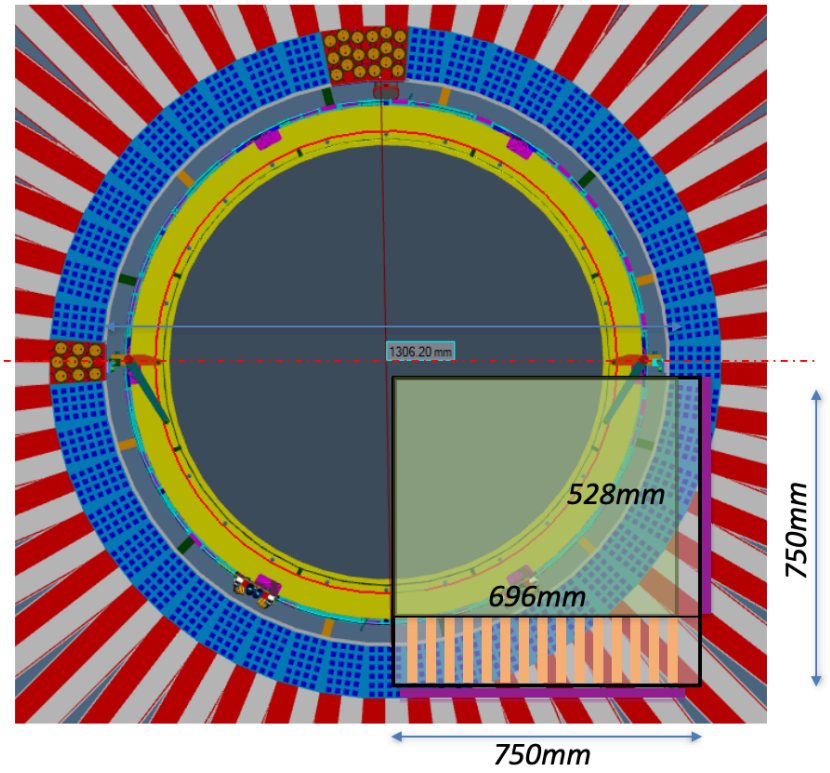

FIG. 7: Front view of the GEM-TRD large-scale prototype that has 696×528 mm^2 sensitive area.

the DIRC detector, see Fig.17a. Fig.6b shows the timing profile of the detector response for electrons with/without radiator and for pions. Event-by-event analyses using a neural network were performed (Fig.8a, Fig.8b) demonstrating a factor of $\approx$ 10 pion rejection capabilities. Such measurements proved the feasibility of using GEM technology for TR detectors and helped to specify the parameters of the next prototype.

The above results were obtained using pion and electron data taken during different running periods. However, very recently we performed tests with TRD prototypes at Fermilab where we had mixed, electron and hadron secondary beams simultaneously. Preliminary analyses of these tests confirmed the results in Fig.6b.

IV. GEM-TRD IMPACT

The GlueX detector has the unique possibility to study J/ψ photoproduction off the proton near threshold in the full kinematic space, where J/ψ is identified by its di-electron decay. Due to the large and uniform acceptance of the GlueX detector, the measured

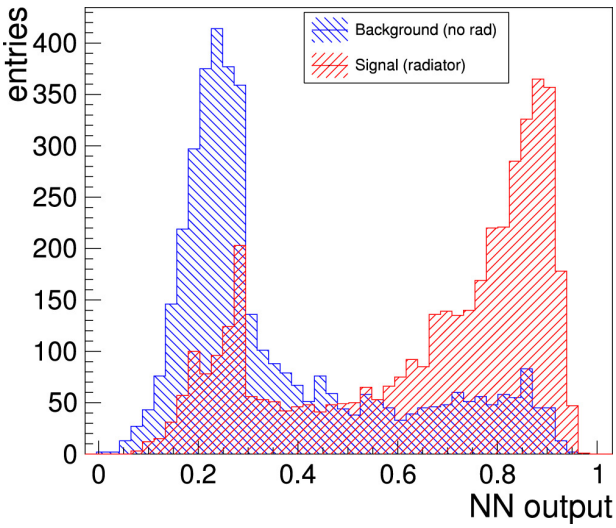

(a) Neural Network (NN) output for electrons with and without radiator

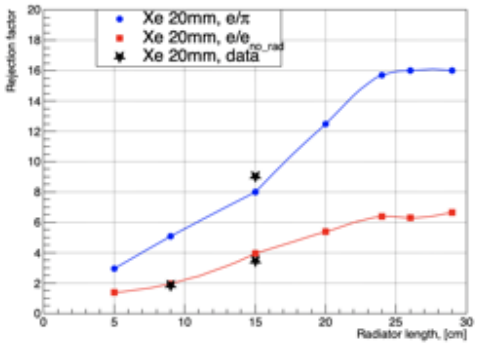

(b) Pion rejection factor from data (stars) and simulations, based on radiator/no radiator (red) and electron/pion (blue) comparison, as function of the radiator thickness. The data are from studies with small prototypes.

FIG. 8

reaction $\gamma p \to pe^+e^-$ includes not only the J/ψ decay but also the non-resonant electromagnetic Bethe-Heitler (BH) process. The BH process can then be used for normalization of the J/ψ cross section. Good electron identification is required to measure the BH process because of a huge $\pi^+\pi^-$ background that can mimic the electron-positron pairs. In current measurements at GlueX, sufficient electron identification is provided by the electromagnetic calorimeters, by applying p/E cuts as discussed below. However, the selected sample of electron-positron pairs still contain a considerable pion contamination (roughly equal amounts of signal to background in the BH region), and the uncertainties related to subtracting this background are the major contribution to the systematic uncertainties in the J/ψ cross section measurements. The main contribution to the overall scale uncertainty comes from the BH normalization (see Table II), which, as it will be discussed below, is directly related to the pion background. The point-to-point systematic errors in the J/ψ yield extraction are also affected by the uncertainties in the efficiency of the p/E cuts. These uncertainties are especially higher around the dip region, see Fig.9. When using only the Phase-I data, most of the data points have statistical errors that are larger than the point-to-point systematic uncertainties. However it is expected that with the full Phase-I and Phase-II data, the systematic errors will have the most significant contribution to the total

source	value
BH data/MC ratio vs $M(e^+e^-)$ and E_γ	15.3%
Radiative corrections	8.3%
TCS contribution to BH	8%
ρ' contribution to BH	3.6%
total	19.5%

TABLE II: Contributions to the overall normalization uncertainty added in quadrature.

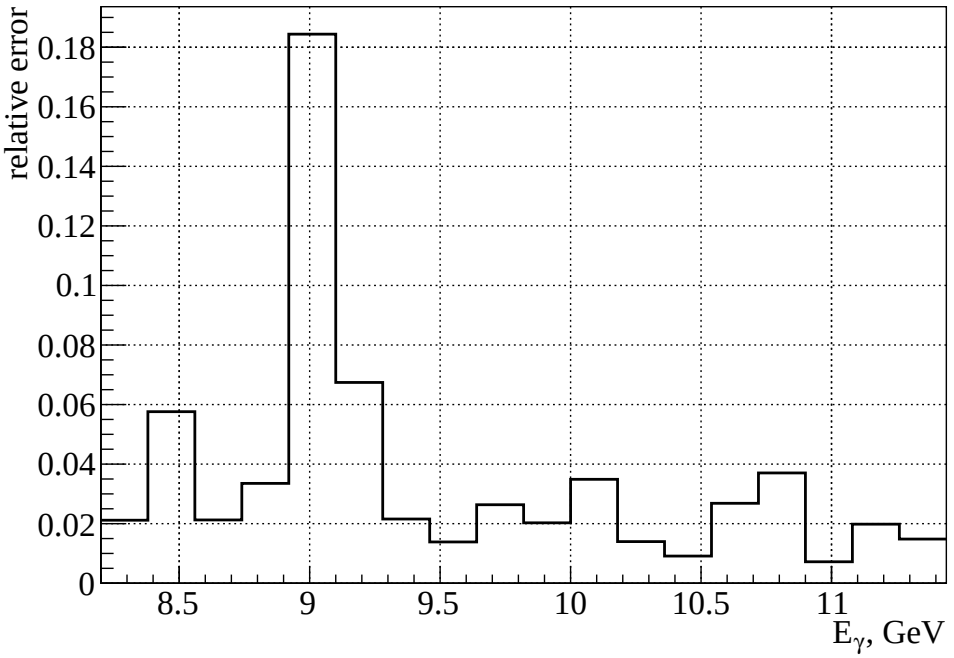

FIG. 9: Relative point-to-point uncertainty from the p/E cuts applied when extracting the J/ψ yields.

uncertainty.

The addition of the proposed GEM-TRD detector has the following advantages:

- As an independent low-mass detector, it can be placed in front of the forward calorimeter allowing to measure precisely the calorimeter's pion suppression efficiency, which is critical for the systematic studies of e^+e^- final states. At the same time the calorimeter can be used to study the efficiency of the GEM-TRD.

- The proposed detector will give a factor of 10 pion suppression allowing the precise measurements of the Bethe-Heitler (BH) electromagnetic process that is fully calculable in QED and has the same e^+e^-p particles in the final state as J/ψ photoproduction.

This will reduce the systematic uncertainties of the latter reaction significantly, particularly the uncertainty on the total normalization will be reduced from 20% to less than 10%.

- The suppression of the pions would allow to estimate the systematic error of one of the most selective cut used in the analyses, the convergence of the kinematic fit.

- The detector will minimize the pion contamination in the J/ψ events to a level at which SDME and amplitude analysis can be performed reliably.

- The GEM-TRD works also as a Time Projection Chamber (TPC) giving a track segment within the drift volume of the detector. This will improve the pattern recognition and the momentum resolution which is limited in the forward direction. At the same time, it will help the performance of the DIRC detector by providing it with a precise tracking measurement close to its face.

A. The effect of pion backgrounds in existing GlueX data

The best approach to extract the absolute J/ψ cross-sections is to use the BH process for normalization using the formula [1, 2]:

$$\sigma = \frac{N_{J/\psi}}{N_{BH}} \frac{\sigma_{BH}}{BR_{J/\psi}} \frac{\varepsilon_{BH}}{\varepsilon_{J/\psi}} , \tag{1}$$

where only the relative efficiency, $\varepsilon_{BH}/\varepsilon_{J/\psi}$, of the J/ψ and BH processes enter, and common overall factors cancel out. In this equation, N_{BH} and $N_{J/\psi}$ are the yields of the corresponding processes, σ_{BH} is the calculated BH cross-section, and $BR_{J/\psi}$ is the branching ratio of the $J/\psi \to e^+e^-$ decay.

Fig.10 illustrates the problem with the pion background in the nominal GlueX detector. This figure shows the e^+e^- invariant mass spectrum from the data (black), compared to simulations that include absolute calculations of the BH process [31–33] in the continuum and the J/ψ peak, the latter normalized to the data (blue). For this plot we apply all the selections as explained in [2]. Most importantly, 3σ cuts are applied around the peaks in the p/E distributions for both the electron and positron candidates (p is the momentum determined by the drift chambers and E the energy deposited in the corresponding calorimeter, BCAL

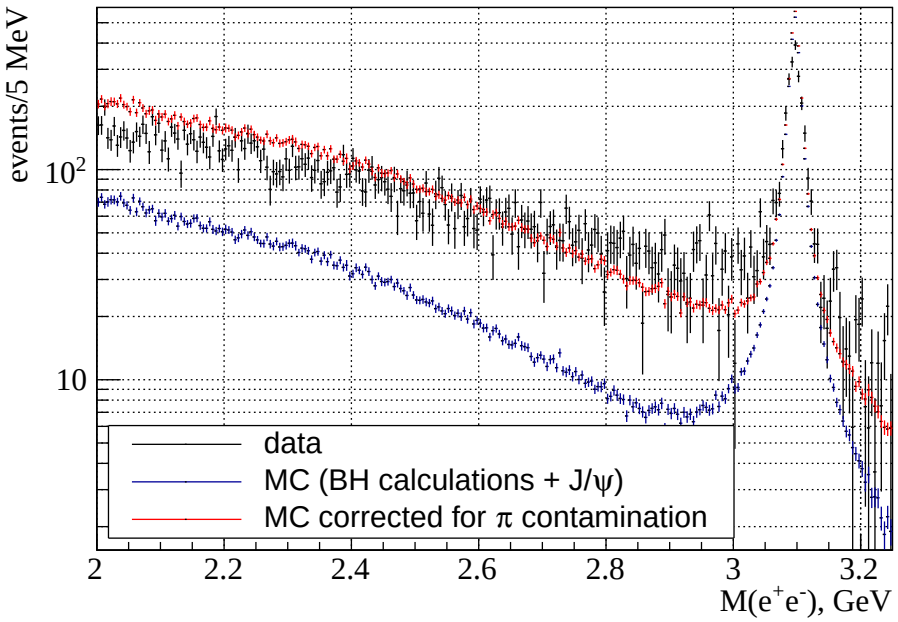

FIG. 10: The e^+e^- invariant mass spectrum from data compared to Monte Carlo simulations that use absolute BH calculations (as well as the J/ψ photoproduction normalized to the data) and their modification that adds the pion background (see text). The invariant mass was deduced from the kinematically fitted lepton momenta.

and FCAL, and their ratio should peak near 1 for electrons and positrons). An additional selection is applied on the signal from the first layer of BCAL, that works as a pre-shower. As we detect all the final state particles and have very good precision for the beam photon energy, we can apply a Kinematic Fit (KF) that constrains the four momenta and the vertex position of the final state particles. The KF significantly reduces the background, as discussed below.

After all these selections are applied, the pion background is of the same order as the signal in the BH region, and we therefore have to use some statistical procedures to estimate the background and extract the BH yields. In practice, we extract the BH yields by fitting the p/E distributions to separate the electron (and positron) contributions. The total of the estimated background plus the BH cross section, is shown by the red points in Fig.10. This corresponds to the simulations (blue) to which the pion background is added using the signal-to-background ratios in Figs.11a,11b. Examples of p/E fits used to estimate these ratios from the data are given in the Appendix.

In Fig.12 we plot the e^+e^- mass spectra for two cases, when at least one lepton goes

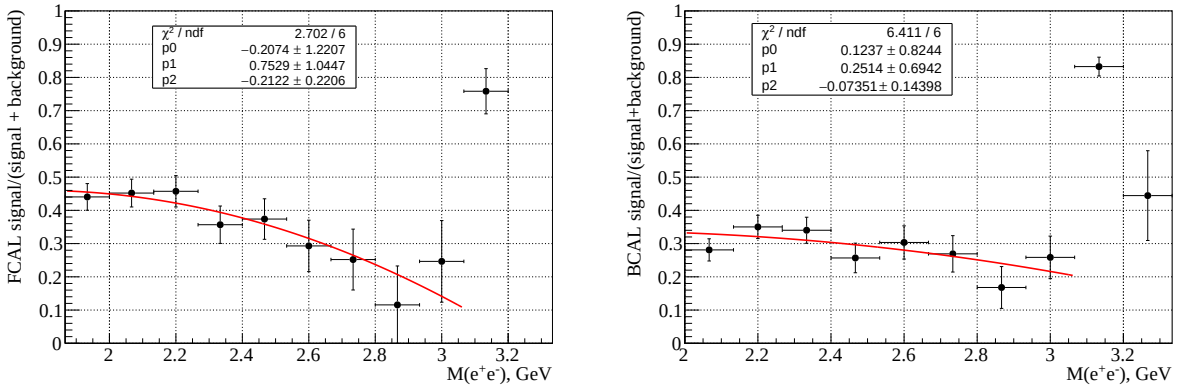

(a) FCAL (b) BCAL

FIG. 11: The signal to (signal+background) ratio as function of the e^+e^- invariant mass, obtained from p/E fits of the data, as explained in the Appendix. The results for the two calorimeters are fitted with polynomials, the latter used to add the pion background in Fig.10.

forward and when both leptons are registered in the BCAL. The pion background is much more significant in the forward direction, where the GEM-TRD will be installed. This can be explained by the fact that background reactions like $\gamma p \to N^*\pi \to p\pi\pi$ (N^* can be any nucleon resonance) will produce predominately one forward pion and one backward pion coming from the target excitation.

B. Electron identification efficiency

As previously described, the p/E cuts are the most important selections in rejecting the pions. However, the simulation of the calorimeter response is not perfect, and these selections may have different efficiencies in data and simulation. The extraction of the BH e^+e^- yield is also sensitive to the shape of the p/E distribution, especially for FCAL due to the steep background (see Appendix).

One can try to do effective corrections to the simulations based on the data, however, due to the complicated momentum and angular dependence of these corrections along with the large pion backgound, this is not possible in practice. The best solution would be to use the GEM-TRD in front of the FCAL to identify a clean sample of electrons and measure the FCAL efficiency in detail as function of the energy and incident angle. The results of these measurements can be used to improve the FCAL electron response in simulation, and

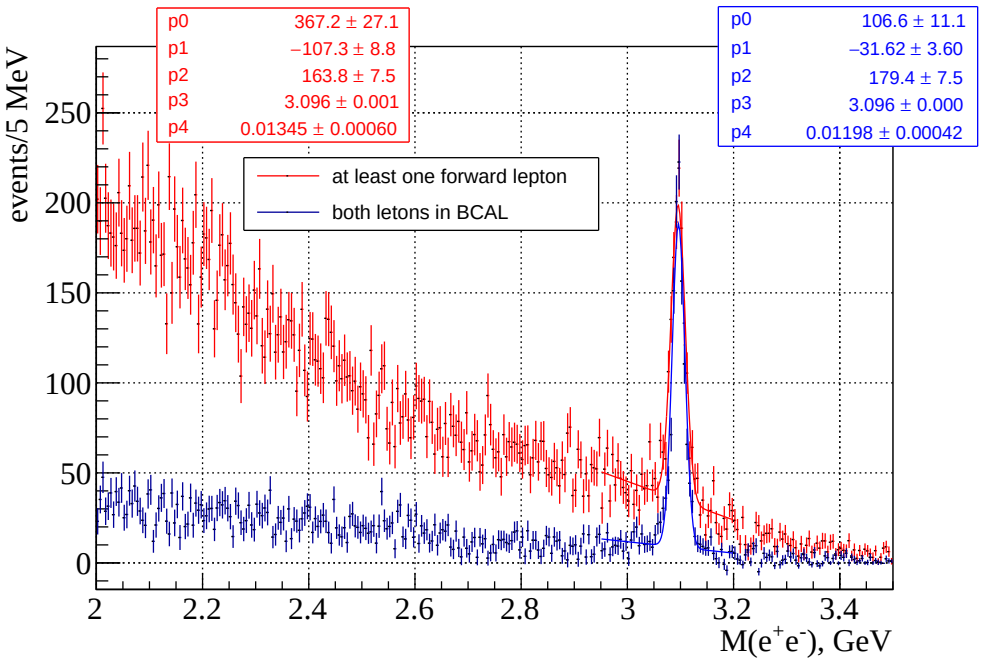

FIG. 12: The e^+e^- invariant mass spectrum from data in case of at least one lepton goes in the forward direction, and when both leptons are registered in BCAL. The background below the J/ψ peak $\pm 3\sigma$ in forward direction is 65%.

improve the systematic error determination for the full data set collected to date.

C. The efficiency of the Kinematic Fit

The Kinematic Fit (KF) cuts more than 50% of the final state particle candidates, therefore potentially it is a significant source of systematic errors depending on how well its efficiency is modeled in simulation. However, the KF is required for this measurement because it improves the e^+e^- mass resolution and reduces the background significantly, especially in the forward direction. To estimate the efficiency of the KF in data, we need to use an alternate analysis method. In particular, we can study the spectrum of the missing mass off of the well-measured proton recoiling off of the J/ψ produced in these exclusive events. Fig.13 shows the e^+e^- mass spectrum as measured by the missing mass off the recoil proton with and without the KF, in the case of at least one lepton in the forward direction. The mass resolution of the J/ψ peak is similar with and without the KF however the background without the KF is significant and prevents the reliable extraction of the J/ψ signal, which limits the precision of this study. Again, the use of the GEM-TRD would reduce the back-

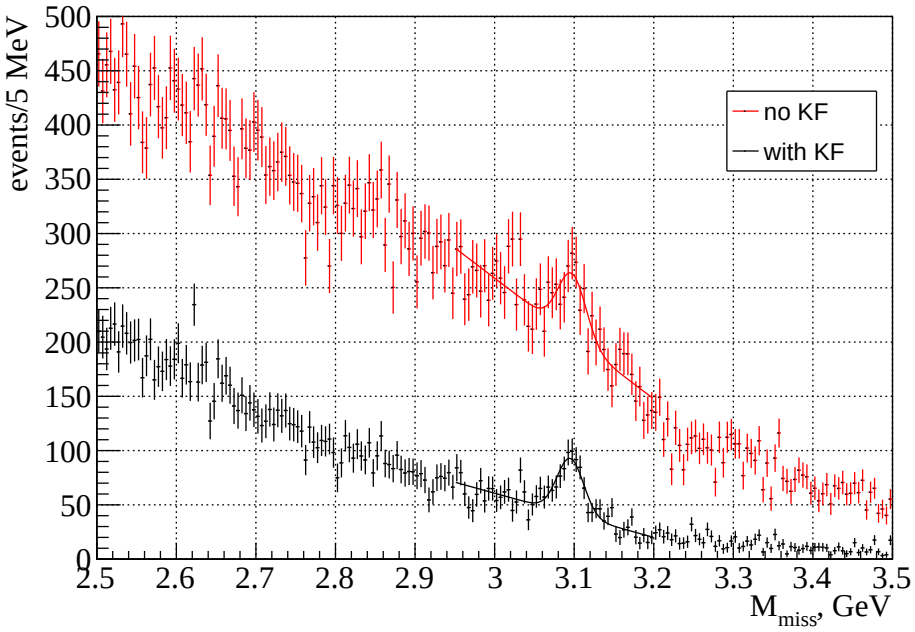

FIG. 13: The missing mass off the recoil proton from the data with and without Kinematic Fit (KF), with at least one forward lepton.

ground under the J/ψ peak to about 10% allowing the measurements of the KF efficiency in this reaction.

D. BH normalization

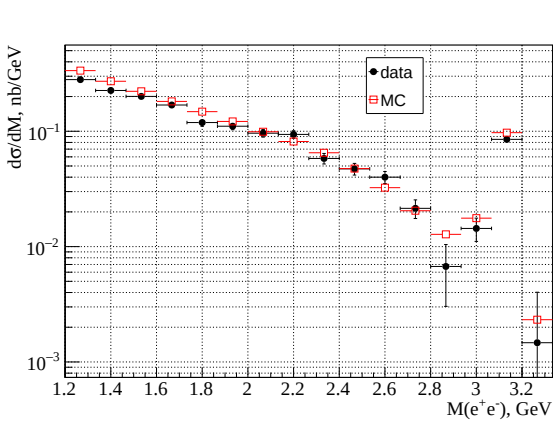

(a) BH cross-sections from data and MC.

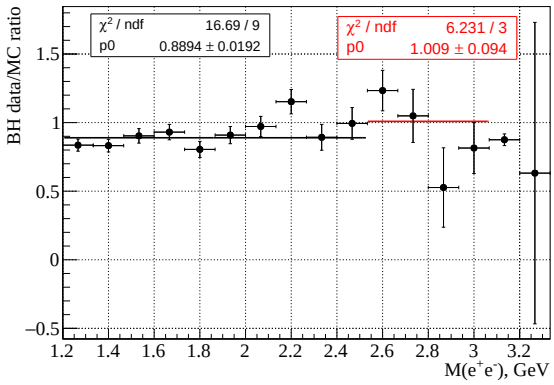

(b) BH data/MC ratio from Fig.14a fitted with constants in two regions.

FIG. 14: BH cross-section vs invariant mass: data vs MC.

The normalization of the J/ψ cross section to the BH process is a key component to the

current measurement. Fig.14 compares the measured BH cross sections to the calculated values as function of the invariant mass. One can see from Fig.14b that the data/MC ratio is not constant and shows a tendency of increasing towards the J/ψ peak, however with a significant uncertainty due to the statistical uncertainties of the procedure. Based on such studies we estimated [2] a contribution to the normalization uncertainty of about 15%, which is the dominant contribution to the systematic uncertainty of the J/ψ cross section. We suspect that the source of this data/MC inconsistency is primarily from the problems discussed in the previous subsections, the poor knowledge of the calorimeter and the KF efficiencies. Additionally, these studies are limited by the statistical errors of the BH yield, which are dominated by the background fluctuations when fitting the p/E distributions (see Appendix).

If we assume negligible pion background, the errors of the BH yield will be significantly smaller as defined simply by the number of events, see Fig.15a. The individual errors of the data points in this case are given in Fig.15b and the fit in the region next to the J/ψ peak gives an uncertainty of 3%. Thus, when including all the contributions to the normalization error [2] (see Table II), the total normalization uncertainty would be expected to fall below 10%.

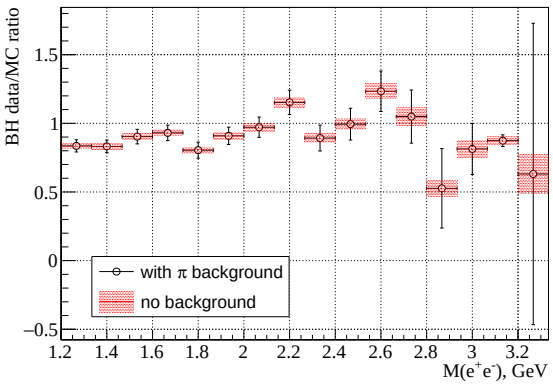

(a) Comparison of errors of the BH data/MC ratio with and without pion background.

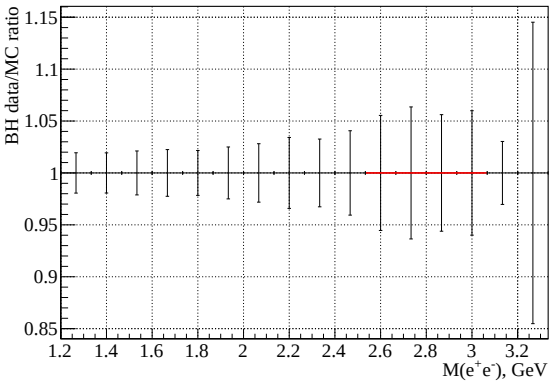

(b) The errors of the data points without background from Fig.15a (value set to unity). The fit with a constant of the points next to the J/ψ peak gives an error of 0.03.

FIG. 15

E. SDME and amplitude analysis

The reduced pion background with the GEM-TRD also opens up the possibility of additional measurements for J/ψ photoproduction.

The linearly polarized photon beam in Hall D allows us to extract the Spin Density Matrix Elements (SDME) of the photoproduction of different mesons. Although statistically limited, a preliminary measurement of these SDMEs for J/ψ photoproduction show some interesting features. The extraction of these quantities however is strongly affected by the presence of pion contamination. The suppression of the pion background is critically important in the clean extraction of the SDMEs and in the estimation of the corresponding systematic errors.

Similarly, performing a full amplitude analysis of the angular distributions from the J/ψ photoproduction requires selection of a clean signal sample. We estimate the GEM-TRD will reduce the pion contamination for the J/ψ events to about 5%, thus permitting a reliable amplitude description of the contributing reactions.

F. Improving the tracking with the GEM-TRD

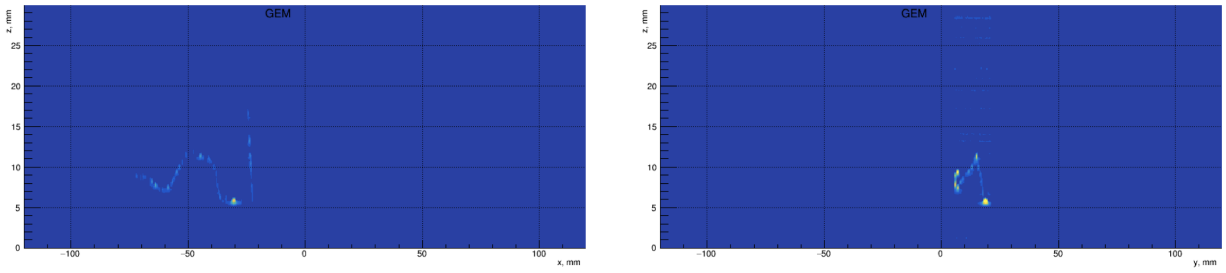

FIG. 16: One event reconstructed with GEM-TRD used as TPC: z vs x (left) and z vs y (right) where z is reconstructed from the drift time.

An important feature of the GEM-TRD detector is that it works also as a Time Projection Chamber (TPC), registering the clusters along the track in the drift volume as function of the drift time. Fig.16 illustrates the precision of this tracking chamber; these results are from a test with a small prototype at the pair spectrometer arm. A tracking system that included the GEM-TRD prototype was installed and tested downstream of the solenoid and in front of the DIRC detector (Fig.17a), just at the place where the final detector will be positioned. The tracks, as reconstructed from the drift chambers inside the magnet, are extrapolated

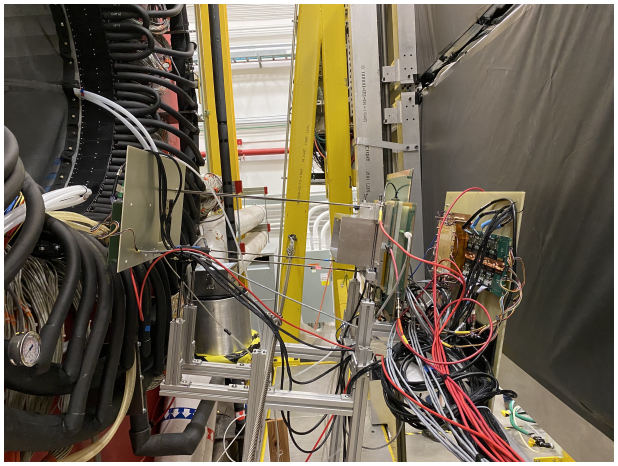

(a) GEM-TRD set-up installed downstream of the magnet (on the left) and in front of the DIRC detector (on the right). It includes pad GEM on the left, wire-TRD, and GEM-TRD on the right with front-end electronics and cables seen on the picture.

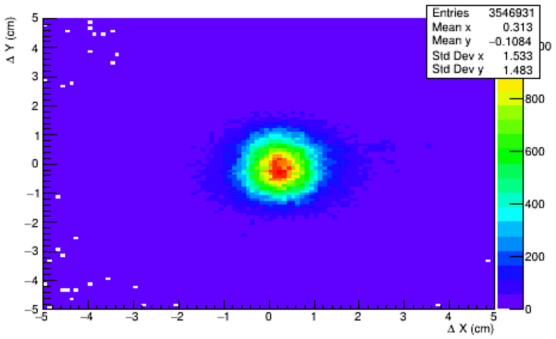

(b) Difference in x and y, between the track extrapolated from drift chambers and the track reconstructed in the GEM-TRD prototype downstream of the magnet.

FIG. 17

to the GEM-TRD and compared with the tracks reconstructed in this detector, Fig.17b. The GEM-TRD will add a tracking segment far away from the GlueX tracking system that has the potential to improve the pattern recognition and the momentum resolution in the forward direction. At the same time, instead of using tracks extrapolated through the magnet's fringe field, the GEM-TRD will give a precise track segment just in front of the DIRC which is of critical importance for the reconstruction of the Cherenkov image in this detector.

G. The effect of the additional material

We realize that adding additional material in front of the FCAL will affect the reconstruction efficiency for the reactions used in the GlueX program, if running simultaneously. The photons will convert to e^+e^- with $< 4\%$ probability and, especially at low energies, the two leptons will end up in FCAL (1 m downstream) close enough to be treated as part of the same shower. To illustrate this we have performed GEANT4 simulations, using a realistic model of the GEM-TRD detector, see Figs.18,19. For comparison the DIRC detector is even thicker (17% R.L.) though closer to FCAL. Nevertheless, as the GEM-TRD has a relatively

small contribution to the total material in front of FCAL, we expect small effect on the reactions of interest for the GlueX program.

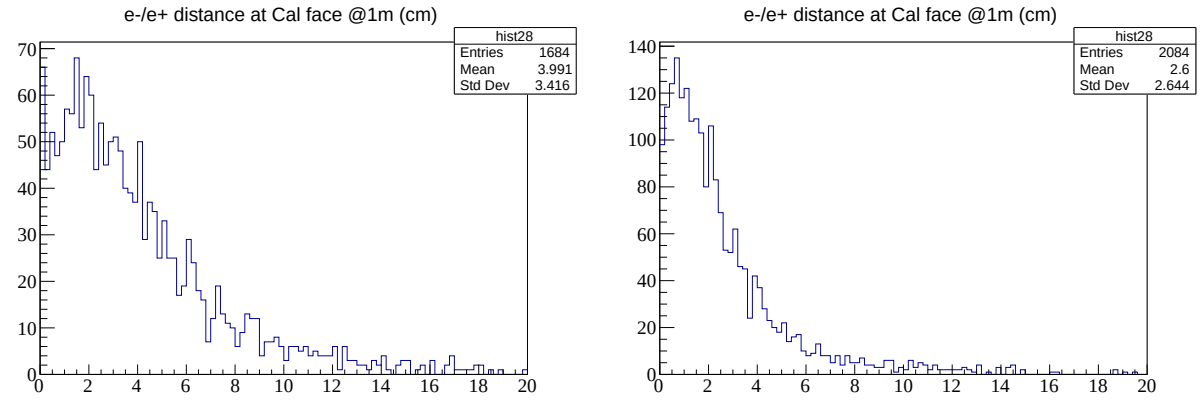

(a) $E_\gamma = 250$ MeV. (b) $E_\gamma = 500$ MeV.

FIG. 18: The distribution of the distance between the two leptons (e^+e^-) on FCAL face for different photon energies.

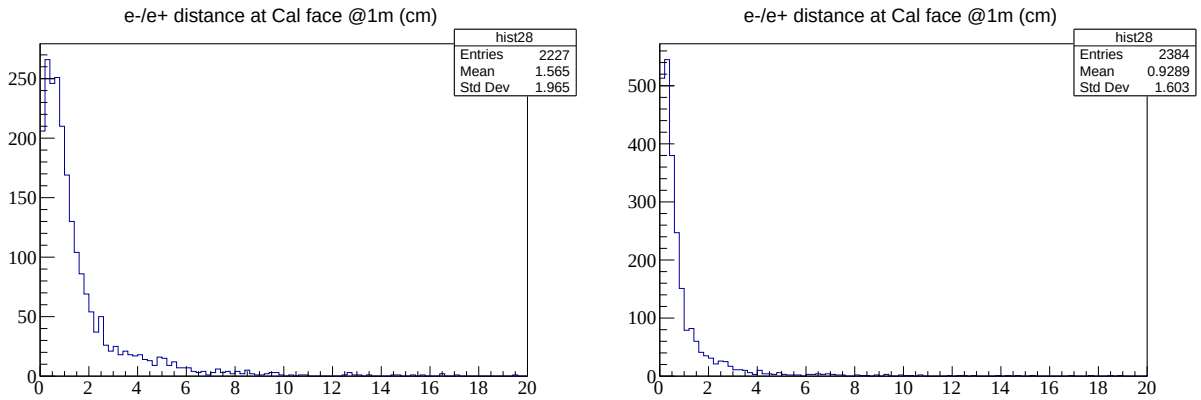

(a) $E_\gamma = 1$ GeV. (b) $E_\gamma = 2$ GeV.

FIG. 19: The distribution of the distance between the two leptons (e^+e^-) on FCAL face for different photon energies.

V. OTHER POTENTIAL IMPROVEMENTS

The study of J/ψ photoproduction in GlueX could also be improved by changing the coherent peak location, the planned FCAL upgrade, and a possible future increase in the experimental luminosity.

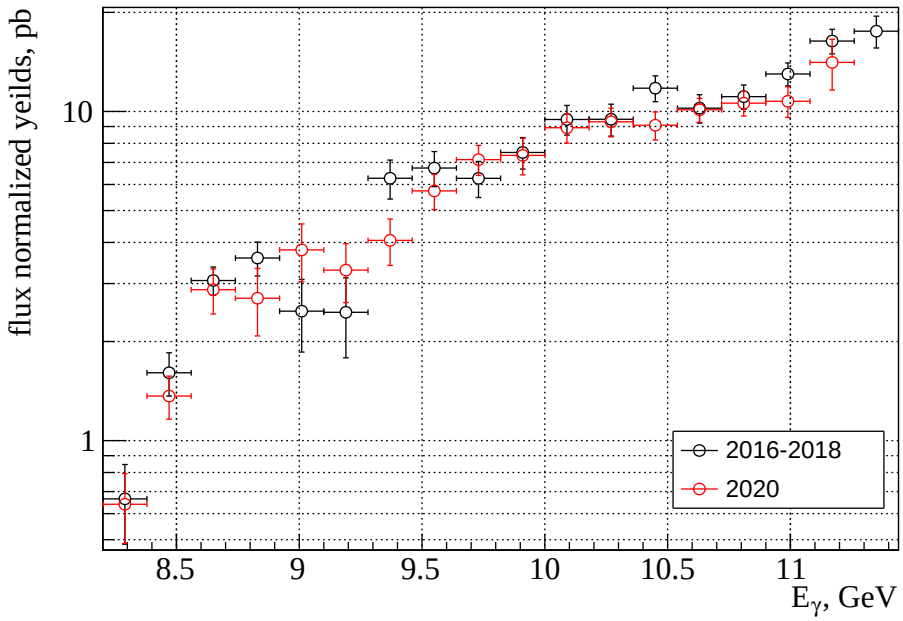

FIG. 20: Comparison of the J/ψ flux-normalized yields for the 2016-2018 and 2020 running periods.

For the first phase of the GlueX experiment the edge of the coherent peak was kept at 8.8 GeV. During the 2020 run, the edge was moved to 8.6 GeV due to the lower electron beam energy. In Figs.20,21 we compare the flux-normalized and the BH-normalized yields for the above two running periods. While a dip in the J/ψ yields at $8.9 - 9.3$ GeV and peak structures at ≈ 8.7 and ≈ 9.4 GeV are seen for the Phase-I data, such structures do not clearly appear in the 2020 data. For comparison, we show in Fig.22 the corresponding photon spectra. For the Phase-I run, the coherent peak and the lower flux next to it seam to follow the structures in the J/ψ energy dependence. While it is tempting to assign the variations in the J/ψ yield to the change in the photon energy spectrum, we note that due to the large statistical uncertainties, the yields from both run periods are consistent and no clear conclusion can be drawn.

To more precisely check the existence of the peak structure at $8.6 - 9.2$ GeV a possible option would be to take advantage of the higher electron beam energy of 12 GeV that is planned for 2024 and beyond, and set the coherent edge at 9.2 GeV. We note that during the engineering run in 2016 when the electron energy was 12 GeV the GlueX experiment had the edge at nominal value of 9 GeV, and expect that this location would be nominally planned for the GlueX run.

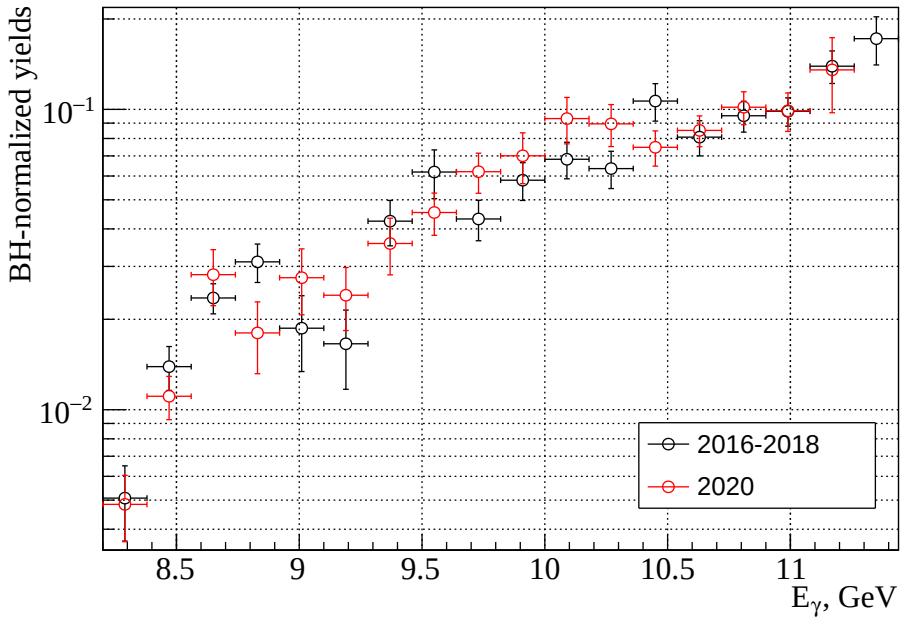

FIG. 21: Comparison of the J/ψ BH-normalized yields for the 2016-2018 and 2020 running periods.

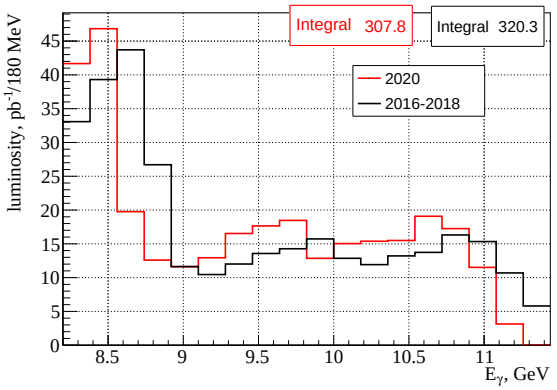

FIG. 22: Comparison of the photon spectra for the 2016-2018 and 2020 running periods.

Therefore, in case we run simultaneously with GlueX, we can estimate the effect of moving the coherent peak up by 200 MeV. In Fig.23a we compare the corresponding photon beam fluxes. Integrating the peaks in the $8.2-9$ GeV and $8.4-9.2$ GeV regions respectively, we see a reduction of the coherent peak flux by 9%. The polarization also drops by 9%, see Fig.23b. This corresponds to a drop of the Figure Of Merit, $FOM = flux \cdot polarization\ squared$, by 23% (Fig.24), which would increase the error of the polarization measurements by 13%.

On the other hand, as seen in Fig.25, the statistical uncertainties in the J/ψ cross section

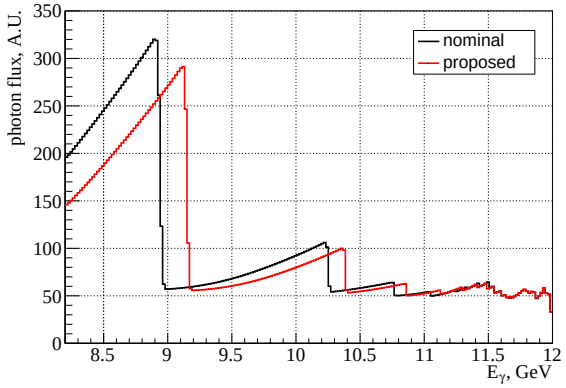

(a) Comparison of the flux for two positions of the coherent peak edge: nominal at 9 GeV and optional at 9.2 GeV.

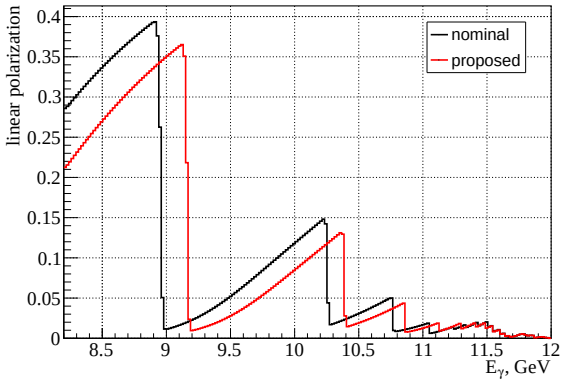

(b) Comparison of the polarization for two positions of the coherent peak edge: nominal at 9 GeV and optional at 9.2 GeV.

FIG. 23

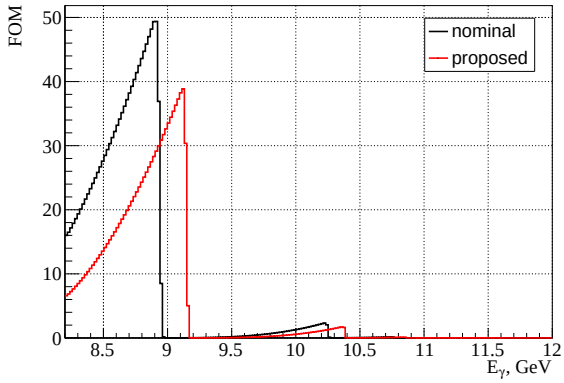

FIG. 24: Comparison of the Figure Of Merit for two positions of the coherent peak edge: nominal at 9 GeV and optional at 9.2 GeV.

points in the $8.9-9.3$ GeV "dip" region are expected to be reduced by $15-50\%$, which will improve our ability to confirm the shape of a possible structure in this region.

The above discussions are based on the assumption that the CEBAF energy will reach 12 GeV by the time of the proposed experiment. A final decision about the position of the coherent peak would naturally be made based on the actual electron beam energy and the needs of the GlueX experiment if running simultaneously.

An important upgrade of the GlueX detector is the new high-resolution FCAL insert, that is being installed now and is planned to be used starting in 2024. The calorimeter consists of 40×40 lead-tungsten crystals occupying the 80×80 cm^2 inner part of FCAL. Due the high J/ψ mass, in this very forward direction only about 8% of the electrons from the J/ψ

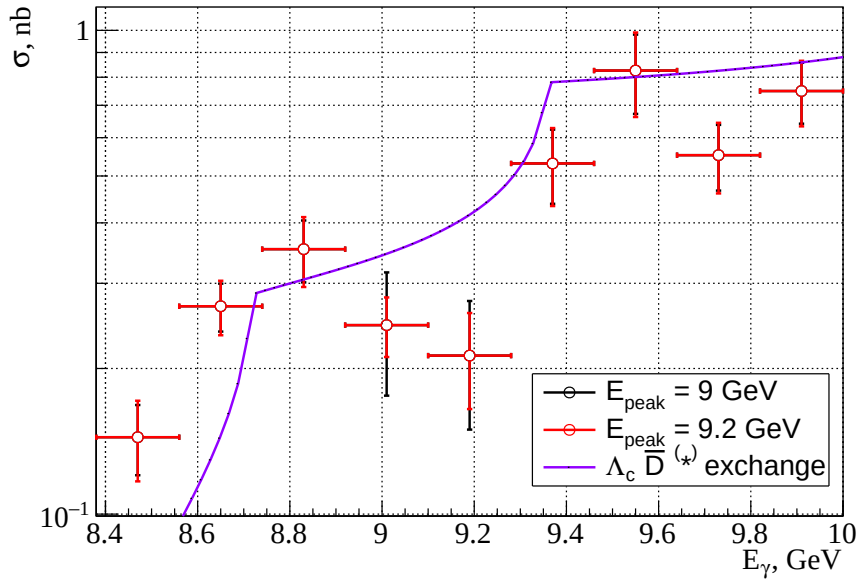

FIG. 25: Comparison of the total cross section errors for two positions of the coherent peak edge: nominal at 9 GeV and optional at 9.2 GeV. Shown is also the result of the theoretical calculations of the open-charm exchange [20].

photoproduction will be detected in this new calorimeter region, predominately for higher beam energies. However, BH process at lower e^+e^- invariant masses will have a significant fraction of the electrons that will end up in this calorimeter. Thus the FCAL insert in combination with the GEM-TRD will help to further characterize the pion background in the continuum region and reduce the systematic uncertainties on the measured cross sections.

Finally, the proposed increase of the intensity of the GlueX experiment by a factor of three [4] would result in significant increase of the statistics that is of critical importance for a more detailed understanding of the J/ψ photoproduction mechanism. The intensity increase would be even more important for the studies of the higher-mass charmonium states, as discussed below, which thresholds are very close to the maximum available photon energy.

VI. BROADER DI-ELECTRON PHYSICS PROGRAM

So far in this document we have discussed the need of using the proposed GEM-TRD detector to reduce the uncertainties in the J/ψ photoproduction measurements. Certainly, this detector which provides an additional order of magnitude pion suppression, can be useful for any reaction with electron-positron pairs in the final state. Here we give one example

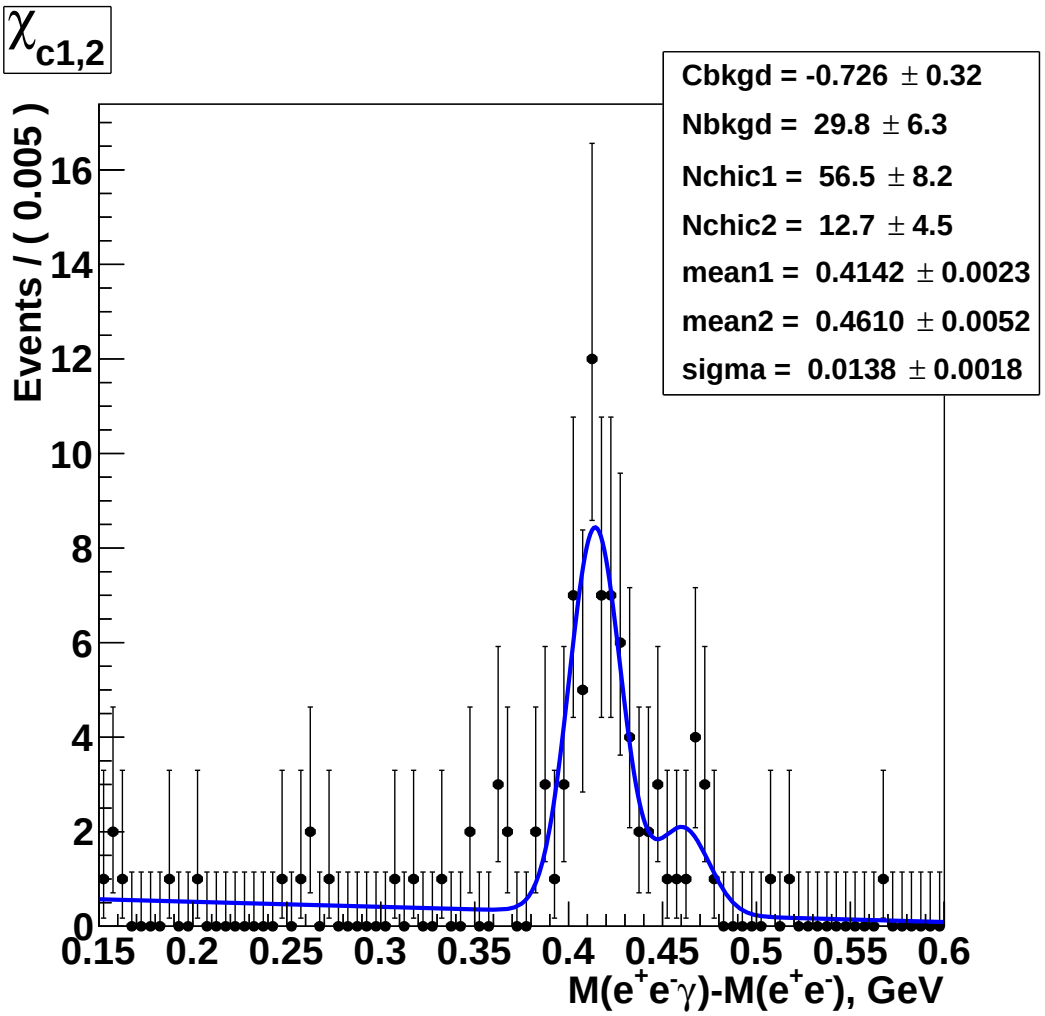

FIG. 26: First ever observation of C-even charmonium in photoproduction: $\chi_{c1(2)}$ detected via their radiative decay $\gamma p \to \chi_{c1(2)} p \to J/\psi \gamma p \to e^+e^-\gamma p$. The corresponding invariant mass difference are fitted with two Gaussians with common width; the mean values match the PDG's mass differences $M_{\chi_{c1(2)}} - M_{J/\psi}$. (GLUEX PRELIMINARY!)

of such studies that are based on results from the GlueX running, and discuss some other future possibilites.

The GlueX experiment has observed a small number of $\chi_{c1(2)}$ charmonium states through their radiative decay to J/ψ, see Fig.26. This is the first ever evidence for photoproduction of C-even charmonium states. Physicists have been looking for such reactions as a direct evidence for odderon exchange, but at higher energies. At H1 at HERA they were searching for odderon exchange in the $\pi^0 N^*$ photoproduction [34] and found no evidence. At threshold energies χ_c could be produced through 3-gluon exchange, but also through other processes such s-channel production or open-charm re-scattering. In Fig.27 we compare the 2D distri-

butions (vs photon energy and t) of χ_c and J/ψ events. We observe a striking difference in the photoproduction of the C-even and C-odd charmonium states. Despite the low statistics, clearly the χ_c distribution is much more flatter than the J/ψ one, the latter showing a typical t-channel concentration of the events close to t_{min}. The thresholds for $\chi_{c1(2)}$ production

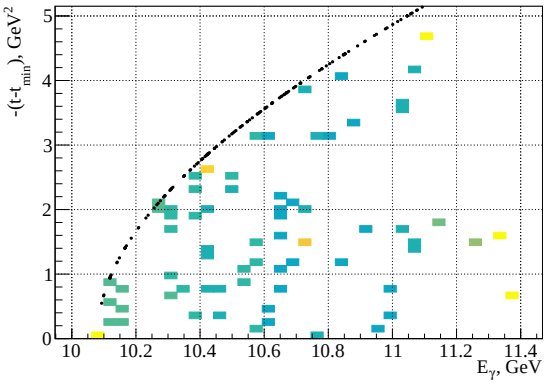

(a) Distribution of the χ_c events within the peak region in Fig.26, as function of beam energy at $-(t - t_{min})$, weighted by the beam photon flux event-by-event. (GLUEX PRELIMINARY!)

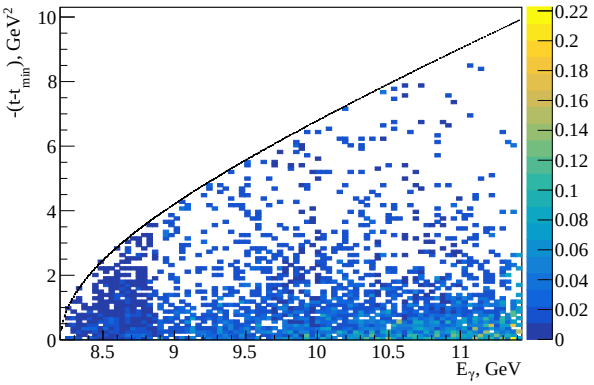

(b) Same as Fig.27a but for the J/ψ photoproduction.

FIG. 27

are ≈ 10 GeV, i.e. close to the end of the GlueX beam photon spectrum. The JLab energy upgrade to 22 GeV is the only feasible path for a precision study of the phenomena of C-even threshold photoproduction and extend the measurements to higher energy, where such an observation could be interpreted as an evidence for a odderon exchange. Nevertheless, this hint of a different production mechanism motivates further studies of the $\chi_{c(1,2)}$ photoproduction with the present 12 GeV accelerator, which would also would be very important in justification of the JLab energy upgrade.

The ability to obtain high purity samples of di-electron events opens up many other aspects of the JLab physics program in Hall D. The Time-like Compton Scattering (TCS) [31], is time-reversal symmetric process to Deeply Virtual Compton Scattering (DVCS) which is studied extensively to probe the three-dimensional spatial structure of the proton at JLab and elsewhere. Hall B published first measurements of the TCS, based on the interference with the BH process in the continuum region of the e^+e^- invariant mass spectrum [35]. They found non-zero beam spin asymmetry and forward-backward asymmetry that are negligible

for the BH process alone. Similar studies with the GlueX data are underway, however they are significantly limited by the pion background.

The study of the decays of the lightest vector ($\omega, \phi, ...$) and pseudoscalar ($\eta, \eta', ...$) mesons (M) into final states containing lepton pairs ($M \to \gamma^* B \to l^+l^- B$, where B can be a photon or another meson) gives access to the electromagnetic transition form factors (TFFs). The latter play an important role in understanding the properties of these strongly interacting particles. Moreover, the study of these TFFs is also crucial for low-energy precision tests of the Standard Model (SM) and Quantum Chromodynamics (QCD). Experimentally, the TFFs can be determined by measuring the actual decay rate of $M \to l^+l^- B$ as a function of the di-lepton invariant mass, normalizing this dependence to the partial decay width $\Gamma(M \to B\,\gamma)$. GlueX has the potential to make important contributions to such studies, with its intense photon beam and large acceptance, but current measurements are limited by the existing electron identification capabilities. The addition of the GEM-TRD detector would be a significant contribution for the studies of these reactions.

VII. SUMMARY

With this document we convey our intent to perform measurements with the GEM-TRD detector in combination with the standard GlueX detector with the main purpose of significantly improving the precision of the measurement of exclusive J/ψ photoproduction, running for a total of 100 PAC days. The experiment can run simultaneously with the GlueX experiment.

Based on measurements with small TRD prototypes and studies with real data from the GlueX phase-I running, we demonstrated that:

- The GEM-TRD is expected to reduce the pion background by an order of magnitude which is needed to facilitate studies of the main systematic uncertainties in the J/ψ photoproduction.

- The GEM-TRD detector will help to reduce the overall scale uncertainty of the J/ψ cross sections down to less than 10% allowing more detailed comparison with the other experiments and common theoretical interpretation of all the available data sets.

- The suppression of the pion contamination will give opportunities for reliable SDME and partial wave analysis of the J/ψ photoproduction.

- The ability to obtain high purity di-electron events opens up many other aspects of the JLab physics program in Hall D with implications for a future JLab energy upgrade. Such program includes studies of higher-mass charmonium states, Timelike Compton Scattering, and electromagnetic Transition Form Factors.

- The GEM-TRD detector will improve the track pattern recognition and the momentum resolution of the GlueX detector.

- The new detector will provide an additional track segment outside of the solenoid that will help to extrapolate the track to the DIRC detector with higher precision, which is a critical input for this detector.

The proposed measurements will certainly benefit from a possible intensity increase of the GlueX experiment, as well as increase of the CEBAF beam energy to 12 GeV, however, these are optional improvements and all the estimates in this document assume nominal conditions.

---

[1] A. Ali et al. (GlueX collaboration), Phys. Rev. Lett. **123**, 072001 (2019).

[2] S. Adhikari et al. (GlueX collaboration), (2023), arXiv:2304.03845 [nucl-ex].

[3] D. Winney, C. Fernandez-Ramirez, A. Pilloni, A. N. H. Blin, M. Albaladejo, L. Bibrzycki, N. Hammoud, J. Liao, V. Mathieu, G. Montana, R. J. Perry, V. Shastry, W. A. Smith, and A. P. Szczepaniak, "Dynamics in near-threshold j/ψ photoproduction," (2023), arXiv:2305.01449 [hep-ph].

[4] J. Stevens for the GlueX collaboration, "A path to the luminosity frontier in Hall D," (2023), Letter of Intent to this PAC51.

[5] D. Kharzeev, H. Satz, A. Syamtomov, and G. Zinovev, Nucl.Phys. A **661**, 568 (1999).

[6] D. Y. Ivanov, A. Schafer, L. Szymanowski, and G. Krasnikov, Eur. Phys. J. C **34**, 297 (2004), [Erratum: Eur.Phys.J.C 75, 75 (2015)], arXiv:hep-ph/0401131.

[7] Y. Guo, X. Ji, and Y. Liu, Phys. Rev. D **103**, 096010 (2021), arXiv:2103.11506 [hep-ph].

[8] Y. Hatta and M. Strikman, Phys. Lett. B **817**, 136295 (2021).

[9] U. Camerini, J. Learned, R. Prepost, C. Spencer, D. Wiser, W. Ash, R. L. Anderson, D. M. Ritson, D. Sherden, and C. K. Sinclair, Phys. Rev. Lett. **35**, 483 (1975).

[10] B. Gittelman, K. M. Hanson, D. Larson, E. Loh, A. Silverman, and G. Theodosiou, Phys. Rev. Lett. **35**, 1616 (1975).

[11] D. Ivanov, P. Sznajder, L. Szymanowski, and J. Wagner, private communication (2022).

[12] P. E. Shanahan and W. Detmold, Phys. Rev. D **99**, 014511 (2019), arXiv:1810.04626 [hep-lat].

[13] Y. Hatta and D.-L. Yang, Physical Review D **98** (2018), 10.1103/physrevd.98.074003.

[14] Y. Hatta, A. Rajan, and D.-L. Yang, Physical Review D **100** (2019), 10.1103/physrevd.100.014032.

[15] K. A. Mamo and I. Zahed, Physical Review D **101** (2020), 10.1103/physrevd.101.086003.

[16] K. A. Mamo and I. Zahed, Physical Review D **103** (2021), 10.1103/physrevd.103.094010.

[17] K. A. Mamo and I. Zahed, "Electroproduction of heavy vector mesons using holographic qcd: from near threshold to high energy regimes," (2021), arXiv:2106.00722 [hep-ph].

[18] L. Frankfurt and M. Strikman, Phys. Rev. D **66**, 031502 (2002).

[19] P. Sun, X.-B. Tong, and F. Yuan, Physical Review D **105** (2022), 10.1103/physrevd.105.054032.

[20] M.-L. Du, V. Baru, F.-K. Guo, C. Hanhart, U.-G. Meiner, A. Nefediev, and I. Strakovsky, The European Physical Journal C **80** (2020), 10.1140/epjc/s10052-020-08620-5.

[21] R. Aaij et al. (LHCb collaboration), Phys. Rev. Lett. **115**, 072001 (2015).

[22] R. Aaij et al. (LHCb collaboration), LHCb-PAPER-2019-014 CERN-EP-2019-058, arXiv:1904.03947 (2019).

[23] Q. Wang, X.-H. Liu, and Q. Zhao, Phys. Rev. D **92**, 034022 (2015).

[24] V. Kubarovsky and M. B. Voloshin, Phys. Rev. D **92**, 031502 (2015).

[25] M. Karliner and J. Rosner, Phys. Lett. B **752**, 329 (2016).

[26] A. Blin, C. Fernandez - Ramirez, A. Jackura, V. Mathieu, V. Mokeev, A. Pilloni, and A. Szczepaniak, Phys. Rev. D **94**, 034002 (2016).

[27] B. Duran, Z. E. Meziani, S. Joosten, M. K. Jones, S. Prasad, C. Peng, W. Armstrong, H. Atac, E. Chudakov, H. Bhatt, D. Bhetuwal, M. Boer, A. Camsonne, J. P. Chen, M. Dalton, N. Deokar, M. Diefenthaler, J. Dunne, L. E. Fassi, E. Fuchey, H. Gao, D. Gaskell, O. Hansen, F. Hauenstein, D. Higinbotham, S. Jia, A. Karki, C. Keppel, P. King, H. S. Ko, X. Li, R. Li,

D. Mack, S. Malace, M. McCaughan, R. E. McClellan, R. Michaels, D. Meekins, L. Pentchev, E. Pooser, A. Puckett, R. Radloff, M. Rehfuss, P. E. Reimer, S. Riordan, B. Sawatzky, A. Smith, N. Sparveris, H. Szumila-Vance, S. Wood, J. Xie, Z. Ye, C. Yero, and Z. Zhao, "When color meets gravity; near-threshold exclusive j/ψ photoproduction on the proton," (2022).

[28] F. Babosa, https://halldweb.jlab.org/doc-private/DocDB/ShowDocument?docid=1364 The GAS-II/GPC-II GlueX Preamp Card Preliminary Test Results (2009).

[29] G. Visser, D. Abbot, F. Barbosa, C. Cuevas, H. Dong, E. Jastrzembski, B. Moffit, and B. Raydo, in *IEEE Nuclear Science Symposuim & Medical Imaging Conference* (IEEE, 2010) pp. 777–781.

[30] F. Barbosa, H. Fenker, S. Furletov, Y. Furletova, K. Gnanvo, N. Liyanage, L. Pentchev, M. Posik, C. Stanislav, B. Surrow, and B. Zihlmann, Nuclear Instruments and Methods in Physics Research Section A: Accelerators, Spectrometers, Detectors and Associated Equipment **942**, 162356 (2019).

[31] E. Berger, M. Diehl, and B. Pire, Eur.Phys.J.C **23**, 675 (2002).

[32] R. Paremuzyan, private communication (2017).

[33] R. Jones, private communication (2018).

[34] C. A. et al. (H1 collaboration), Phys. Rev. B **544**, 35 (2002).

[35] P. Chatagnon et al. (CLAS collaboration), Phys. Rev. Lett. **127**, 262501 (2021).

VIII. APPENDIX

Examples of the p/E fits in bins of the e^+e^- invariant mass are given in Fig.28 for BCAL and in Fig.29 for FCAL.

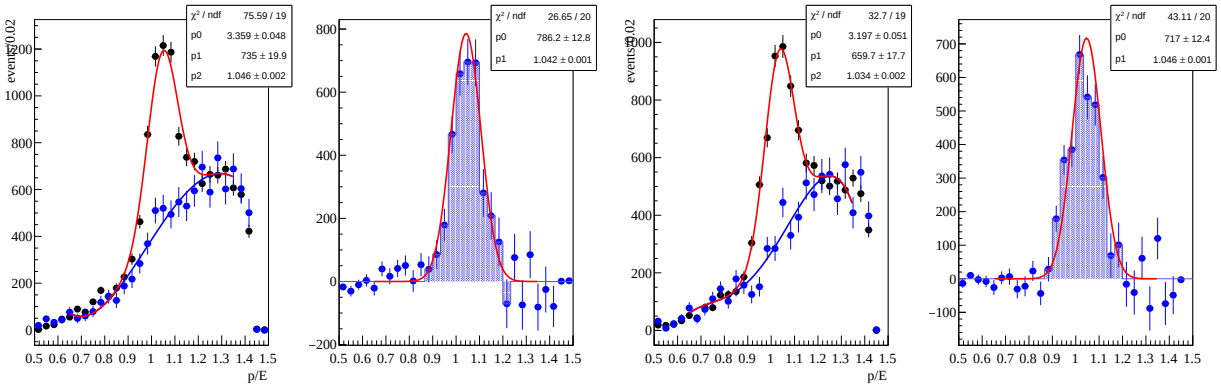

(a) BCAL $1.73 < M(e^+e^-) < 2$ GeV

(b) BCAL $2 < M(e^+e^-) < 2.27$ GeV

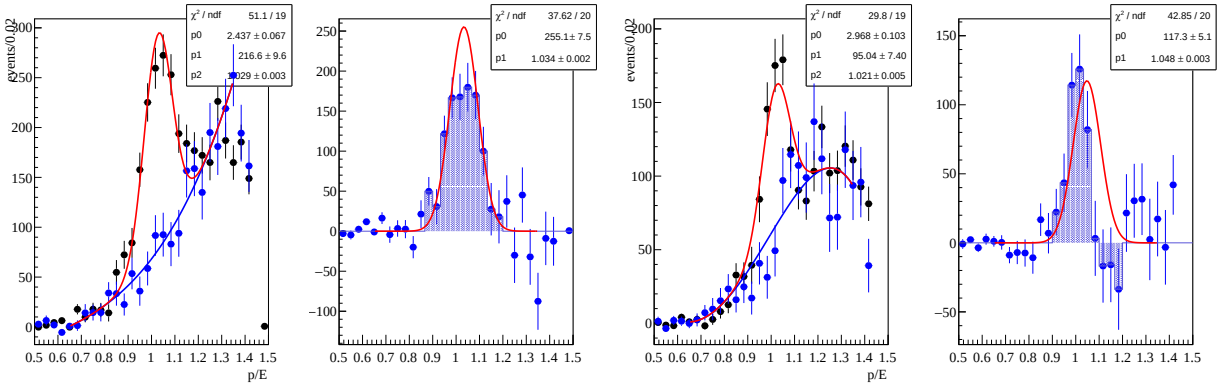

(c) BCAL $2.53 < M(e^+e^-) < 2.8$ GeV

(d) BCAL $2.8 < M(e^+e^-) < 3.07$ GeV

FIG. 28: Fits of p/E distributions for BCAL for four bins in $M(e^+e^-)$. In the left panel of each plot the blue points fitted with the blue curve represent the background distribution (from the sideband of the p/E distribution of the other lepton), while the total distribution is shown with black points fitted with a Gaussian (fixed σ) plus the background polynomial (p0-p4 parameters); the three fitted parameters are the normalization coefficients of the Gaussian and the polynomial and the mean of the Gaussian. The right panel is the difference between the black and blue points from the left panel, fitted with a Gaussian with fixed width (p0, p1 - amplitude and mean); the sum of the shaded points ($\pm 3\sigma$) is used as an estimate of the signal.

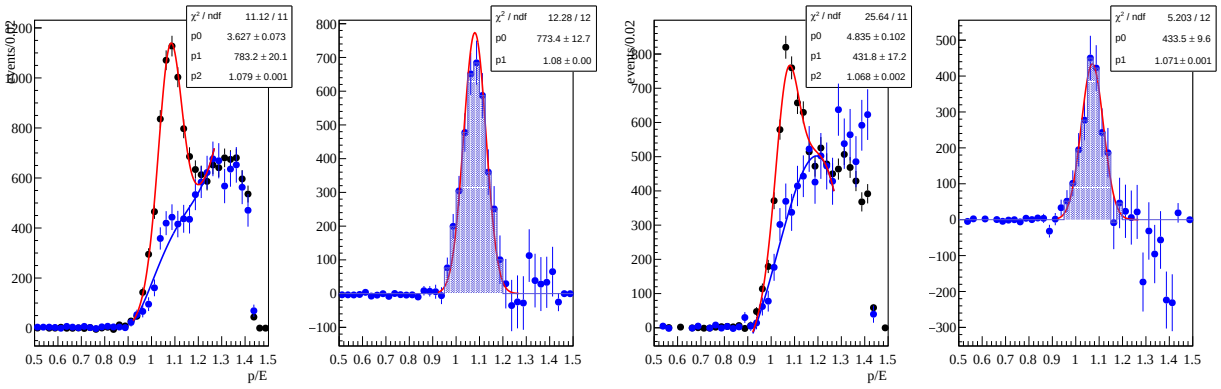

(a) FCAL $1.73 < M(e^+e^-) < 2$ GeV

(b) FCAL $2 < M(e^+e^-) < 2.27$ GeV

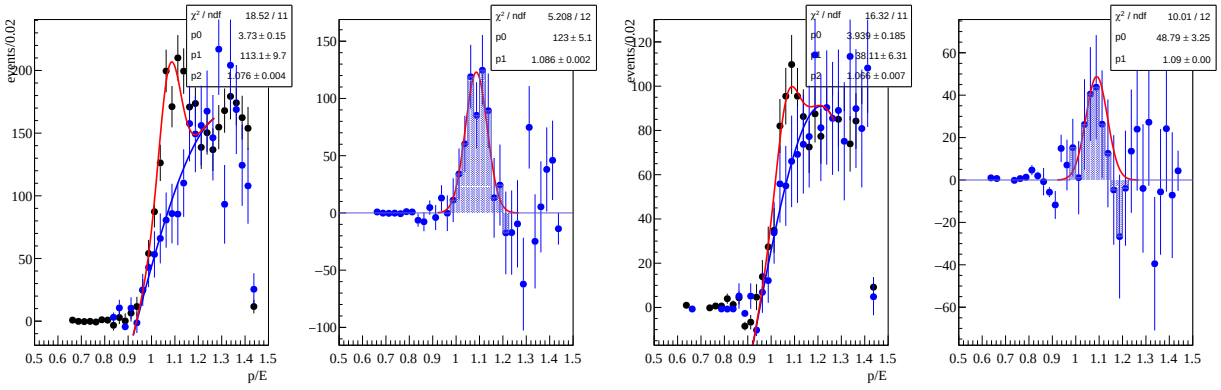

(c) FCAL $2.53 < M(e^+e^-) < 2.8$ GeV

(d) FCAL $2.8 < M(e^+e^-) < 3.07$ GeV

FIG. 29: Same as in Fig.28 but for FCAL.